ANCC FLOW: ADAPTIVE NORMALIZED CROSS-CORRELATION WITH EVOLVING GUIDANCE AGGREGATION FOR DENSE CORRESPONDENCE ESTIMATION

Seungryong Kim[†] *Dongbo Min*[‡] *Kwanghoon Sohn*[†]

[†]School of Electrical and Electronic Engineering, Yonsei University, Seoul, Korea
[‡]Department of Computer Science and Engineering, Chungnam National University, Daejeon, Korea
E-mail: khsohn@yonsei.ac.kr

ABSTRACT

Adaptive normalized cross-correlation (ANCC) cost function works well between images under photometric distortions, but its heavy computational burden often limits its applications. To overcome this limitation, this paper proposes a robust and efficient computational framework, called *ANCC flow*, designed for establishing dense correspondences between images under severe photometric variations. We first simplify the weight of ANCC in an asymmetric manner by considering a source image weight only. It is then efficiently computed by applying constant-time edge-aware filters without loss of its matching accuracy. Additionally, to deal with a large discrete label space effectively, which is a challenging issue in flow field estimations, we propose a randomized label space sampling strategy similar to PatchMatch filer (PMF) optimization. The robustness of the asymmetric ANCC and the cost filter is further enhanced through an evolving weight computation, where a flow field computed in a previous iteration is utilized to build current edge-aware weights. Experimental results demonstrate the outstanding performance of ANCC flow in many cases of dense correspondence estimations under severe photometric and geometric variations.

Index Terms— adaptive normalized cross-correlation, Patchmatch filter, dense correspondence, stereo matching

1. INTRODUCTION

In many computer vision and computational photography applications, images captured under different imaging modalities are popularly used to overcome their inherent limitations, such as flash and no-flash images [1], color and dark flash images [2], blurred images [3, 4], and images under different radiometric conditions [5].

To realize these tasks, establishing dense correspondences between image pairs across photometric variations is an essential problem. Conventional methods for estimating depth [6] or optical flow [7, 8] fields, in which input images are acquired in a similar imaging condition, have been dramatically advanced in recent studies. In these approaches, a matching fidelity term is not a critical issue, as they assume that multiple images share a similar visual pattern. Instead, they focus on powerful labeling optimizers, *e.g.,* graph-cut (GC) [9], PatchMatch [10], cost volume filter [11], non-rigid dense correspondence (NRDC) [12], and Patchmatch filter (PMF) [13]. However, for images taken under different modality conditions, they cannot deal with severe photometric variations without suitable matching cost functions or descriptors [14]. In those cases, robust cost functions designed to deal with modality variations are one of the most important issues to yield a reliable matching quality [15]. Unfortunately, conventional gradient-based descriptors such as scale invariant feature transform (SIFT) [16] and DAISY [17], as well as intensity comparison-based binary descriptors such as binary robust independent elementary features (BRIEF) [18], have shown a limited performance in matching under photometric variations [15].

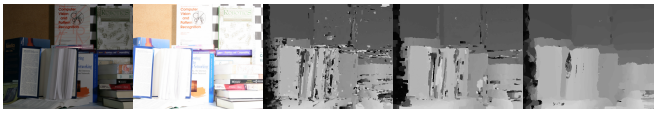

(a) (b) (c) (d) (d)

Fig. 1. Comparison of ANCC flow with existing approaches. (a), (b) stereo images, and depth maps with (c) NCC+GC, (c) ANCC+GC, and (d) ANCC flow. ANCC flow runs $60\times$ faster than ANCC+GC while providing a lower error rate (5.11% vs. 12.24%).

To overcome these limitations, a number of methods have been proposed, and could be categorized as feature-based and area-based approaches. In feature-based approaches, several methods tried to reformulate existing descriptors [19], but they showed limitations similar to existing descriptors. Schechtman and Irani introduced local self-similarity (LSS) descriptor [20], and achieved impressive results in object detection and retrieval. Based on the LSS [20], several methods applied it to multi-modal registration problems [21, 22, 23, 15]. These feature-based approaches have shown satisfactory results in a robust manner, but their discriminative power is limited, leading to difficulty of accurate matches especially on boundary regions.

Among area-based approaches, mutual information (MI)-based cost function is used for a registration of multi-modal medical images [24]. As a pioneering work, the cross-correlation (CC)-based cost function has been popularly used for multi-modal image correspondences, *e.g.,* normalized CC (NCC) [6], adaptive NCC (ANCC) [25], Mahalanobis distance CC (MDCC) [26], and robust selective normalized CC (RSNCC) [27]. Although they provide satisfactory results, when the search space is large, their computational time is also inevitably high [15]. When incorporated with an global energy function and solved by a global optimizer [9], their complexity further dramatically increases.

In this paper, our approach is focusing on the ANCC cost function [25], which has shown satisfactory results on correspondences under photometric variations, but has inherently high computational burdens. We reformulate ANCC [25] in a robust and efficient manner, and further combine it with a cost volume filtering-based optimization [11, 13]. Specifically, our approach approximates ANCC [25] by considering a source guidance weight only, which enables us to apply constant time edge-aware filters (EAF) [28] for a fast computation. To reduce a computational burden for large search spaces, we further employ PMF-like random search strategy. In the optimization procedure, by leveraging evolving guidance weights in computing the cost function and cost volume filter, more reliable

and robust flow fields are estimated as the iterations. Unlike other methods, our ANCC flow can be easily extended to overcome geometric variation problems between image pairs. In experiments for image pairs under photometric and even geometric variations, our ANCC flow outperforms conventional feature-based and area-based approaches both quantitatively and qualitatively.

2. THE ANCC COST FUNCTION AND ITS LIMITATIONS

Let us define an image as $f_i : \mathcal{I} \rightarrow \mathbb{R}$ for pixel $i = [x_i, y_i]^T$, where $\mathcal{I} \subset \mathbb{N}^2$ is a discrete image domain. Given a pair of images f_i^s and f_i^t, a dense correspondence estimation aims to assign each pixel i a label $l_i \in \mathcal{L} = \{l = [u_l, v_l]^T\}$, satisfying that $f^s_{i+l_i} = f_i^t$.

Unlike conventional cost measures [6], an adaptive normalized cross-correlation (ANCC) cost function deals with photometric variations between multiple images effectively, by leveraging its edge-aware subtraction and normalization [25]. Given a pixel i and its label candidate l, the ANCC cost function $\Phi(i,l)$ is defined between two patches $\mathcal{F}_i$ for pixel i of source image f^s and $\mathcal{F}_j$ for corresponding pixel j (where $j = i - l_i$) of target image f^t as

$$\Phi(i,l) = \frac{\sum_{i',j'} \omega_{i,i'}\omega_{j,j'} \left(f_{i'} - \mathcal{G}_i\right)\left(f_{j'} - \mathcal{G}_j\right)}{\sqrt{\sum_{i'} \left\{\omega_{i,i'}(f_{i'} - \mathcal{G}_i)\right\}^2}\sqrt{\sum_{j'} \left\{\omega_{j,j'}(f_{j'} - \mathcal{G}_j)\right\}^2}}, \tag{1}$$

where $i' \in \mathcal{F}_i$ and $j' \in \mathcal{F}_j$, and weighted averages on $\mathcal{F}_i$ and $\mathcal{F}_j$ are defined such that $\mathcal{G}_i = \sum_{i'} \omega_{i,i'} f_{i'}$ and $\mathcal{G}_j = \sum_{j'} \omega_{j,j'} f_{j'}$, $\omega_{i,i'}$ is the normalized adaptive weight of a support pixel i' defined on the image. Based on the cost $\Phi(i,l)$ for all pixel i and all candidate $l \in \mathcal{L}$, the final flow fields are generally inferred by minimizing the energy function with a global optimizer, *e.g.* graph-cut (GC) [9].

Although it provides outstanding performances, it has inherent limitations to be applied to a general dense correspondence scenario. Due to its computation of edge-aware weights $\omega_{i,i'}$ and $\omega_{j,j'}$, a computational time dramatically increases as a large size of support window $|\mathcal{F}|$ and search space $|\mathcal{L}|$ [25]. Furthermore, the edge-aware weight defined on a color image only leads to texture copy problems from the color image [29] and building non-reliable cost volumes, which limits the matching performance.

3. THE ANCC FLOW

3.1. Overview of Our Approach

Our ANCC flow formulates a more robust energy function for flow field estimations by intelligently combining the ANCC cost function [25] and cost volume filter [11], which is solved very efficiently in an unified computational framework (Sec. 3.2). Unlike conventional ANCC [25], our approach first approximates it as only considering a source guidance image, which enables us to apply fast EAF very efficiently without performance loss (Sec. 3.3.1). Under constructed cost volumes, a cost volume filtering for the optimization is followed (Sec. 3.3.2), where the weights for adaptive support aggregation is also re-used as one from the cost computation. To overcome a computational bottleneck from a large label search space, we propose the PMF-like search space sampling scheme. In each iteration, estimated flow fields is considered as a new guidance image for the asymmetric ANCC cost computation and the cost filtering, which simultaneously enhances a matching quality and boosts a convergence (Sec. 3.3.2). Fig. 2 illustrates the ANCC flow framework.

3.2. Our Computational Model

Similar to cost volume filter [11] or PMF [13], we employ a local window-based cost aggregation scheme to provide a reliable matching performance with a very low computational time. In particular,

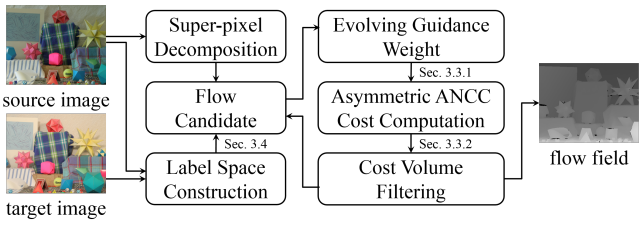

Fig. 2. Framework of ANCC flow. Through an asymmetric ANCC, PatchMatch filter-like optimization, and evolving guidance aggregations, it computes a reliable flow field very efficiently.

to infer l_i for pixel i, our approach first builds a more robust cost volume using asymmetric ANCC cost function such that

$$\mathcal{C}(i,l) = \sum\nolimits_{i' \in \mathcal{F}_i} \omega^l_{i,i'} \left(1 - \tilde{\Phi}^l\left(i', l\right)\right), \tag{2}$$

where $\mathcal{F}_i$ is local neighborhood for cost aggregation, which is same as that in (1), and it is computed for all $i \in \mathcal{I}$ and $l \in \mathcal{L}$.

With the cost volume $\mathcal{C}(i,l)$, final flow field can be estimated as winner takes-all (WTA) optimization as follows:

$$l_i = \text{argmin}_{l \in \mathcal{L}} \mathcal{C}(i,l). \tag{3}$$

In contrast to existing cost filtering-based methods [11, 13], our computational model is mainly different in two aspects. First, asymmetric ANCC cost function $\tilde{\Phi}^l(i,l)$ is utilized, which features that it only considers a source guidance weight function with evolving guidance settings. Namely, the edge-aware weights are computed using the previously estimated flow field, which will be described in Sec. 3.3.1. Second, cost $\mathcal{C}(i,l)$ is aggregated by a cost filter with evolving guidance weight $\omega^l_{i,i'}$, which will be described in Sec. 3.3.2. Note that an evolving guidance concept is first introduced in [30], where its robustness is investigated in the image filtering. Our approach is first attempt to apply it in stereo matching.

Our computational model for ANCC flow is designed so that very efficient computation is feasible. A straightforward computation of (2) might be extremely time-consuming, because its complexity depends on $|\mathcal{F}|$ and $|\mathcal{L}|$. In the following, we introduce an efficient computation scheme for minimizing the energy in (2).

3.3. Efficient Computational Solver

To reduce the computational dependency of $|\mathcal{F}|$, we first reformulate ANCC as a source guided version, which enables us to apply fast EAF [28]. Similar to PMF [13], to reduce the computational dependency of $|\mathcal{L}|$, our approach adopts the superpixel-based inference model for computing cost and cost volume filter, simultaneously.

3.3.1. Asymmetric ANCC cost computation with evolving guidance

To efficiently handle large computational burden for weights in (1), we simplify it by considering only the weights $\omega_{i,i'}$ from the source patch $\mathcal{F}_i$ so that a fast computation using a fast EAF is feasible. It should be noted that such an asymmetric weight approximation has been also used in cost aggregation for stereo matching [11].

Our asymmetric ANCC cost function is first defined as

$$\tilde{\Phi}(i,l) = \frac{\sum_{i',j'} \omega_{i,i'}(f_{i'} - \mathcal{G}_i)(f_{j'} - \mathcal{G}_{i,j})}{\sqrt{\sum_{i'} \omega_{i,i'}(f_{i'} - \mathcal{G}_i)^2}\sqrt{\sum_{j'} \omega_{i,i'}(f_{j'} - \mathcal{G}_{i,j})^2}}, \tag{4}$$

where $\mathcal{G}_{i,j} = \sum_{i',j'} \omega_{i,i'} f_{j'}$, which means a weighted average of $f_{j'} \in \mathcal{F}_j$ with a guidance image $f_{i'} \in \mathcal{F}_i$.

Algorithm 1: The ANCC Flow Framework

Input : image pair f_i^s and f_i^t.
Output : dense correspondence field $l_i \in \mathcal{L}$.
1 : Define the label space $\mathcal{L}$ as in Sec. 3.4
2 : Decompose the image f_i^s into superpixels $\mathbf{S}_f$.
3 : Assign an initial label l^* randomly to each superpixels $\mathcal{S}_m$.
while not converged **do**
  for $m = 1 : M$ **do**
4 : Propagate a set of labels $\mathcal{L}_p$ randomly sampled from neighboring segments to the segment $\mathcal{S}_m$.
5 : Compute $\mathcal{G}_i^{l^*}$ and $\mathcal{G}_{i^2}^{l^*}$ for all pixel i.
for $l \in \mathcal{L}_p$ **do**
6 : Construct a cost slice f_j such that $j = i - l_i$.
7 : Compute $\mathcal{G}_{i,ij}^{l^*}$, $\mathcal{G}_{i,j}^{l^*}$, and $\mathcal{G}_{i,j^2}^{l^*}$ with l^*.
8 : Estimate $\tilde{\Phi}^{l^*}(i,l)$ using (4).
9 : Estimate $\mathcal{C}(i,l)$ using (2) with l^*.
end for
10 : Update an intermediate flow l^* with WTA in (3).
11 : Randomly sample $q \in \mathcal{S}_m$ for defining $\mathcal{L}_q$.
12 : Update $\mathcal{C}(i,l)$ by following Step $\mathbf{6}-\mathbf{9}$ for all $l \in \mathcal{L}_q$.
13 : Update an intermediate flow l^* with WTA in (3).
  end for
end while

With some arithmetic derivations, (4) can be decomposed as

$$\frac{\mathcal{G}_{i,ij} - \mathcal{G}_i \cdot \mathcal{G}_{i,j}}{\sqrt{\mathcal{G}_{i^2} - \mathcal{G}_i^2} \cdot \sqrt{\mathcal{G}_{i,j^2} - \mathcal{G}_{i,j}^2}}, \tag{5}$$

where $\mathcal{G}_{i^2} = \sum_{i'} \omega_{i,i'} f_{i'}^2$, $\mathcal{G}_{i,ij} = \sum_{i',j'} \omega_{i,i'} f_{i'} f_{j'}$, and $\mathcal{G}_{i,j^2} = \sum_{i',j'} \omega_{i,i'} f_{j'}^2$. Similar to efficient computation scheme in [15], (5) can be computed very efficiently using a constant-time EAF [31, 28].

Furthermore, to improve a robustness and discriminative power, our final cost function makes use of an evolving guidance aggregation in a way that the previously estimated flow field is considered as a guidance for the adaptive support aggregation in (5) such that

$$\tilde{\Phi}^l(i,l) = \frac{\mathcal{G}_{i,ij}^l - \mathcal{G}_i^l \cdot \mathcal{G}_{i,j}^l}{\sqrt{\mathcal{G}_{i^2}^l - (\mathcal{G}_i^l)^2} \cdot \sqrt{\mathcal{G}_{i,j^2}^l - (\mathcal{G}_{i,j}^l)^2}}, \tag{6}$$

where $\mathcal{G}_{i,ij}^l$, $\mathcal{G}_{i^2}^l$, $\mathcal{G}_{i,j^2}^l$, $\mathcal{G}_i^l$, and $\mathcal{G}_{i,j}^l$ are computed with $\omega_{i,i'}^l$, which is defined as edge-aware weights from previously estimated label l.

3.3.2. PMF based cost optimization

Our asymmetric ANCC cost in (6) can be computed very efficiently compared to original ANCC in (1), but its computational time still depends on search range size $|\mathcal{L}|$. To overcome this limitation, we employ label search space sampling strategy in PMF [13]. In the optimization, for the evolving guidance aggregation, our approach utilizes the previous flow field to construct edge-aware weights. We first decompose the image f as superpixel $\mathbf{S}_f = \{\mathcal{S}_m | \bigcup_m \mathcal{S}_m = \mathcal{I} \text{ and } \forall m \neq n,\ \mathcal{S}_m \bigcap \mathcal{S}_n \neq \varnothing,\ m \in 1, ..., M\}$, where M is the number of superpixels. A random label is initially assigned to each node, and we iterate two search strategies in an interleaved manner, *i.e., neighborhood propagation* and *random search*.

In *neighborhood propagation* step, for a current segment $\mathcal{S}_m$, we denote its set of spatially adjacent neighbors as $\{\mathcal{S}_k\}$, and candidate pixels $p \in \mathcal{S}_k$ are then randomly sampled from every neighboring segment. A set of current best labels $\mathcal{L}_p = \{l_p\}$ is then retrieved. For $l \in \mathcal{L}_p$, an asymmetric ANCC cost in (5) and cost volume filtering in (2) are computed sequentially. After the preceding propagation step, in *random search* step, we randomly pick a reference pixel $q \in \mathcal{S}_m$ to promote the label propagation within a segment. After defining a set of labels $\mathcal{L}_q = \{l_q\}$, (5) and (2) are computed again for pixels $i \in \mathcal{S}_m$. After each iteration, the intermediate flow field is inferred using (3), and is applied to next iteration as an evolving guidance aggregation, which will boost matching performances on each iteration. Algorithm 1 summarizes our ANCC flow.

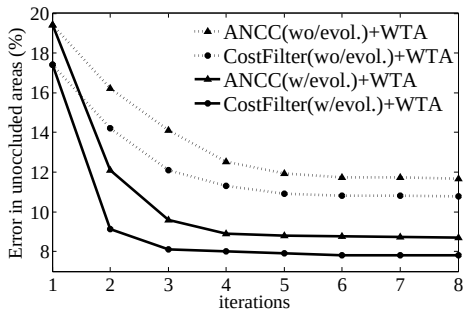

Fig. 3. Convergence analysis of the ANCC flow. By employing a evolving guidance aggregation, its matching performance is highly improved and boosted as increasing the iterations.

image size	SIFT flow	NCC w/GC	ANCC w/GC	ANCC flow†	ANCC flow‡
463×370	$32.1s$	$30.2s$	$305.1s$	$235.2s$	$\mathbf{5.1}s$

Table 1. Evaluation of computational complexity. The brute-force and efficient computation of our ANCC flow are denoted as † and ‡, respectively. Our approach runs $60\times$ faster than ANCC w/ GC.

3.3.3. Effects of evolving guidance aggregation

Fig. 3 shows convergence analysis of ANCC flow. In order to analyze only effects of evolving guidance aggregations in cost computation and cost aggregation, not PMF itself [13], disparity maps from the cost computation with WTA and its corresponding cost filtering with WTA are estimated with fixed $\mathcal{L}_p$ and $\mathcal{L}_q$. As shown in Fig. 3, an evolving guidance aggregation dramatically improves matching performances in cost computation and cost filtering, simultaneously. It further enables boosting very fast convergence.

3.4. Extension to Geometric-Invariant Flow Field Estimation

By properly defining the search label space $l_i \in \mathcal{L}$, our ANCC flow can be applied to general dense correspondence problems. For stereo matching, l_i is defined to assign a disparity d ($u_l = d$) to pixel i, where $v = 0$. For optical flow estimation, l_i is defined to assign a 2-D vector field for $[u_l, v_l]$. More challengingly, for general image matching scenarios, where there exist not only translation fields but also geometrically variations fields, *e.g.,* scale and rotation, it is hard to directly define l_i due to too many possible candidates. Instead, we employ a randomized global transform approach [32]. Specifically, based on initial sparse feature matching and RANSAC-based global transform inference [33], we estimate global transform candidates $\mathbf{T}_c$ between multiple images, which can deal with scale and rotation field very efficiently. Using $\mathbf{T}_c$, search label spaces are defined in such a way that $l_i = \mathbf{T}_c(i)$ for all c, where $\mathbf{T}_c(i)$ means that pixel i is applied by global transform $\mathbf{T}_c$. In this case, $|\mathcal{L}| = |\mathbf{T}_c|$.

3.5. Computational Complexity Analysis

Given an image size $|\mathcal{I}|$, the label space size $|\mathcal{L}|$, the number of iteration K, and the aggregation window size $|\mathcal{F}|$, the computational complexity the ANCC flow framework on the brute-force implementation becomes $O(K|\mathcal{I}||\mathcal{L}|4|\mathcal{F}|)$. With efficient computation model with fast constant-time EAF, our approach removes the complexity dependency on the aggregation window size $|\mathcal{F}|$, *i.e.,* $O(K|\mathcal{I}||\mathcal{L}|)$.

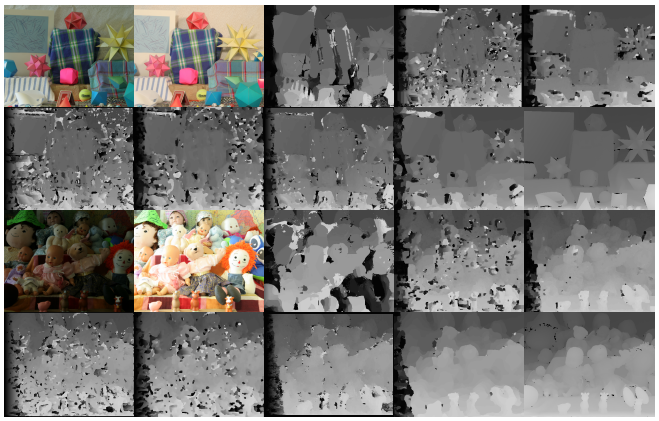

Fig. 4. Comparison of disparity estimations for image pairs across illumination '1/3' and exposure '0/2' [6]. (from top to bottom) image pairs, depth maps from cost filter [11], NCC [6], ANCC [34], SIFT [16], DAISY [17], DASC [15], ANCC flow, and ground truth.

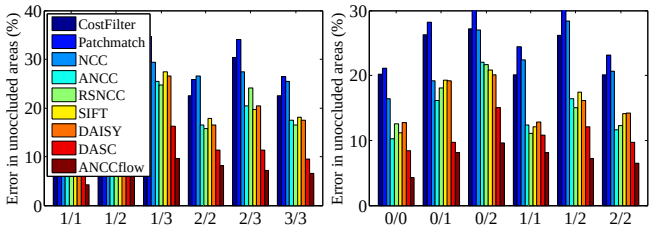

(a) illumination variation (b) exposure variation

Fig. 5. Average bad-pixel error rate on the Middlebury benchmark [6] with (a) illumination and (b) exposure variations.

Furthermore, by employing PMF-like inference model to reduce the effect of large search spaces, our final computational complexity can be dramatically reduced to $O(|\mathcal{I}|\log|\mathcal{L}|)$.

4. EXPERIMENTAL RESULTS AND DISCUSSION

4.1. Experimental Environments

In experiments, the ANCC flow was implemented with the following same parameter settings for all datasets. For an EAF, we employed the guided filter (GF) [28] with radius $r = 9$ and the smoothness parameter $\varepsilon = 0.009$. The number of superpixels is set to about 500 using the SLIC [35]. We implemented the ANCC flow in C++ on Intel Core i7-3770 CPU at 3.40 GHz. The computational complexity of ANCC flow compared to other methods was evaluated in Table 1.

ANCC flow was compared to state-of-the-art matching methods, *e.g.,* cost filter [11], PatchMatch [10], and SIFT [16], DAISY [17], and DASC [15] combined with SIFT flow [36] optimization. Furthermore, we compared our approach with NCC [6] and ANCC [34] with GC [9] optimization. For geometric-invariant flow estimations, we evaluated SID [37], SegSID [37], and SSF [38].

4.2. Middlebury Stereo Benchmark

We first evaluate our ANCC flow framework in Middlebury stereo benchmark containing illumination and exposure variations [6]. In the experiments, the illumination (or exposure) combination '1/3' indicates that two images were captured under the 1^{st} and 3^{rd} illumination (exposure) conditions. For a quantitative evaluation, we measured the bad-pixel error rates in non-occluded areas [6].

Fig. 4 shows depth maps for severe illumination and exposure variations, and Fig. 5 shows average bad matching error rates. As expected, without robust cost functions, the cost filter [11] and PatchMatch [10] cannot provide reliable correspondence performances. Matching performances of SIFT flow [36] combined with robust cost functions [17, 18, 20, 15] are limited on edge-discontinuity regions since they provide limited discriminative power. Furthermore, their computational time was very high. Unlike these conventional methods, our ANCC flow achieved the best results both quantitatively and qualitatively. By using an leveraging guidance aggregation, the matching performance of ANCC flow was highly enhanced.

	ANCC w/GC	SIFT flow	SID	SegSID	SSF	ANCC flow
LTA	39.2	34.2	39.1	34.0	29.7	**16.3**

Table 2. Average LTA error rates on DIML benchmark [15].

(a) (b) (c) (d) (e)

Fig. 6. Comparison of qualitative evaluation on DIML benchmark [15]. (a),(b) image pairs, warped color images from correspondences of (c) SIFT flow [36], (d) SID [37], and (e) ANCC flow.

4.3. DIML Benchmark

We then evaluate our ANCC flow framework in recently published DIML benchmark [15], captured as 10 geometry image sets by combining geometric variations of viewpoint, scale, and rotation, and each image set consists of images taken under 5 different photometric variation pairs including illumination, exposure, flash-noflash, blur and noise. To evaluate the performance quantitatively, we computed the label transfer accuracy (LTA) [39, 15].

Fig. 6 shows qualitative evaluation results, and Table 2 shows average LTA error rates for all combinations. SIFT flow-based approaches [17, 18, 20, 15] cannot provide reliable matching qualities under geometric variations. Geometry-invariant methods, such as SID [37], SegSID [37], and SSF [38], showed robustness to geometric variations to some extent, but they showed limited performance on photometric variations. Contrarily, through optimally defined flow field candidates, our ANCC flow provided the robustness for both photometric and geometric variations.

5. CONCLUSION

The adaptive normalized cross-correlation (ANCC) flow framework has been proposed for establishing dense correspondences between images taken under different imaging modalities. Its high performance of a matching quality and a computational time in comparison to state-of-the-art approaches can be attributed to greater robustness of asymmetric ANNC cost with evolving guidance aggregations, PMF-like optimization, and its efficient computational scheme. The ANCC flow has been validated on an extensive set of experiments that cover photometric and geometric variations. In future work, it can be applied to challenging non-rigid image deformations.

6. REFERENCES

[1] G. Petschnigg, M. Agrawals, and H. Hoppe, "Digital photography with flash and no-flash iimage pairs," *In Proc. of ACM SIGGRAGH*, 2004.

[2] D. Krishnan and R. Fergus, "Dark flash photography," *In Proc. of ACM SIGGRAGH*, 2009.

[3] Y. HaCohen, E. Shechtman, and E. Lishchinski, "Deblurring by example using dense correspondence," *In Proc. of ICCV*, 2013.

[4] H. Lee and K. Lee, "Dense 3d reconstruction from severely blurred images using a single moving camera," *In Proc. of CVPR*, 2013.

[5] P. Sen, N. K. Kalantari, M. Yaesoubi, S Darabi, D. B. Goldman, and E. Shechtman, "Robust patch-based hdr reconstruction of dynamic scenes," *In Proc. of ACM SIGGRAGH*, 2012.

[6] D. Scharstein and R. Szeliski, "A taxonomy and evaluation of dense two-frame stereo correspondence algorithms," *IJCV*, vol. 47, no. 1, pp. 7–42, 2002.

[7] D. Butler, J. Wulff, G. Stanley, and M. Black, "A naturalistic open source movie for optical flow evaluation," *In Proc. of ECCV*, 2012.

[8] D. Sun, S. Roth, and M. Black, "Secret of optical flow estimation and their principles," *In Proc. of CVPR*, 2010.

[9] Y. Boykov, O. Yeksler, and R. Zabih, "Fast approximation enermgy minimization via graph cuts," *IEEE Trans. PAMI*, vol. 23, no. 11, pp. 1222–1239, 2001.

[10] C. Barnes, E. Shechtman, D. B. Goldman, and A. Finkelstein, "The generalized patchmatch correspondence algorithm," *In Proc. of ECCV*, 2010.

[11] C. Rhemann, A. Hosni, M. Bleyer, C. Rother, and M. Gelautz, "Fast cost-volume filtering for visual correspondence and beyond," *In Proc. of CVPR*, 2011.

[12] Y. HaCohen, E. Shechtman, D. B. Goldman, and D. Lischinski, "Non-rigid dense correspondence with applications for image enhancement," *In Proc. of ACM SIGGRAGH*, 2011.

[13] J. Lu, H. Yang, D. Min, and M. N. Do, "Patchmatch filter: Efficient edge-aware filtering meets randomized search for fast correspondence field estimation," *In Proc. of CVPR*, 2013.

[14] P. Pinggera, T. Breckon, and H. Bischof, "On cross-spectral stereo matching using dense gradient features," *In Proc. of BMVC*, 2012.

[15] S. Kim, D. Min, B. Ham, S. Ryu, M. N. Do, and K. Sohn, "Dasc: Dense adaptive self-correlation descriptor for multi-modal and multi-spectral correspondence," *In Proc. of CVPR*, 2015.

[16] D.G. Lowe, "Distinctive image features from scale-invariant keypoints," *IJCV*, vol. 60, no. 2, pp. 91–110, 2004.

[17] E. Tola, V. Lepetit, and P Fua, "Daisy: An efficient dense descriptor applied to wide-baseline stereo," *IEEE Trans. PAMI*, vol. 32, no. 5, pp. 815–830, 2010.

[18] M. Calonder, "Brief : Computing a local binary descriptor very fast," *IEEE Trans. PAMI*, vol. 34, no. 7, pp. 1281–1298, 2011.

[19] S. Saleem and R. Sablatnig, "A robust sift descriptor for multi-spectral images," *IEEE SPL*, vol. 21, no. 4, pp. 400–403, 2014.

[20] E. Schechtman and M. Irani, "Matching local self-similarities across images and videos," *In Proc. of CVPR*, 2007.

[21] A. Torabi and G. Bilodeau, "Local self-similarity-based registration of human rois in pairs of stereo thermal-visible videos," *Pattern Recognition*, vol. 46, no. 2, pp. 578–589, 2013.

[22] Y. Ye and J. Shan, "A local descriptor based registration method for multispectral remote sensing images with non-linear intensity differences," *ISPRS J. Photogram. Remote Sens.*, vol. 90, no. 7, pp. 83–95, 2014.

[23] S. Kim, S. Ryu, B. Ham, B. Kim, and K. Sohn, "Local self-similarity frequency descriptor for multispectral feature matching," *In Proc. of ICIP*, 2014.

[24] J. Pluim, J. Maintz, and M. Viergever, "Mutual information based registration of medical images: A survey," *IEEE Trans. MI*, vol. 22, no. 8, pp. 986–1004, 2003.

[25] Y. Heo, K. Lee, and S. Lee, "Robust stereo matching using adaptive normalized cross-correlation," *IEEE Trans. PAMI*, vol. 33, no. 4, pp. 807–822, 2011.

[26] S. Kim, B Ham, B Kim, and K. Sohn, "Mahalanobis distance cross-correlation for illumination invariant stereo matching," *IEEE Trans. CSVT*, vol. 24, no. 11, pp. 1844–1859, 2014.

[27] X. Shen, L. Xu, Q. Zhang, and J. Jia, "Multi-modal and multi-spectral registration for natural images," *In Proc. of ECCV*, 2014.

[28] K. He, J. Sun, and X. Tang, "Guided image filtering," *IEEE Trans. PAMI*, vol. 35, no. 6, pp. 1397–1409, 2013.

[29] J.S. Park, H.W. Kim, Y.W. Tai, M.S. Brown, and I.S. Kweon, "High quality depth map upsampling for 3d-tof cameras," *In Proc. of ICCV*, 2011.

[30] Q. Zhang, X. Shen, L. Xu, and J. Jia, "Rolling guidance filter," *In Proc. of ECCV*, 2014.

[31] E. Gastal and M. Oliveira, "Domain transform for edge-aware image and video processing," *In Proc. of ACM SIGGRAGH*, 2011.

[32] K. Park, S. Kim, S. Ryu, and K. Sohn, "Randomized global transformation approach for dense correspondence," *In Proc. of BMVC*, 2015.

[33] Q. Tran, T. Chin, G. Carneiro, M. S. Brown, and D. Suter, "In defence of ransac for outlier rejection in deformable registration," *In Proc. of ECCV*, 2012.

[34] Y. Heo, K. Lee, and S. Lee, "Joint depth map and color consistency estimation for stereo images with different illuminations and cameras," *IEEE Trans. PAMI*, vol. 35, no. 5, pp. 1094–1106, 2013.

[35] R. Achanta, A. Shaji, K. Smith, A Lucchi, P. Fua, and S. Susstrunk, "SLIC superpixels compared to state-of-the-art superpixel methods," *TPAMI*, vol. 34, no. 11, pp. 2274–2282, 2012.

[36] C. Liu, J. Yuen, and A. Torralba, "Nonparametric scene parsing via label transfer," *IEEE Trans. PAMI*, vol. 33, no. 12, pp. 2368–2382, 2011.

[37] I. Kokkinos and A. Yuille, "Scale invariance without scale selection," *In Proc. of CVPR*, 2008.

[38] W. Qiu, X. Wang, X. Bai, A. Yuille, and Z. Tu, "Scale-space sift flow," *In Proc. of WACV*, 2014.

[39] J. Kim, C. Liu, F. Sha, and K. Grauman, "Deformable spatial pyramid matching for fast dense correspondences," *In Proc. of CVPR*, 2013.